This is an open access article published under an ACS AuthorChoice License, which permits copying and redistribution of the article or any adaptations for non-commercial purposes.

ACS OMEGA

Article

Cite This: ACS Omega 2018, 3, 18811−18820

http://pubs.acs.org/journal/acsodf

Novel Luminescent Ionic Adducts Based on Pyrene-1-sulfonate

Maria Angela Castriciano,*[,†] Paola Cardiano,[‡] Enza Fazio,[§] Placido Giuseppe Mineo,[∥,⊥,#] Angelo Nicosia,[∥] Roberto Zagami,[†] Mariachiara Trapani,[†] Luigi Monsù Scolaro,[‡] and Sandra Lo Schiavo*[,‡]

[†]CNR-ISMN, Istituto per lo Studio dei Materiali Nanostrutturati, c/o Dipartimento di Scienze Chimiche, Biologiche, Farmaceutiche ad Ambientali, University of Messina, V.le F. Stagno D'Alcontres 31, 98166 Messina, Italy

[‡]Dipartimento di Scienze Chimiche, Biologiche, Farmaceutiche ad Ambientali and [§]Dipartimento di Scienze Matematiche e Informatiche, Scienze Fisiche e Scienze della Terra, University of Messina, V.le F. Stagno D'Alcontres 31, Vill. S. Agata, 98166 Messina, Italy

[∥]Dipartimento di Scienze Chimiche, University of Catania, V. A Doria 6, 95100 Catania, Italy

[⊥]CNR-IPCB Istituto per i Polimeri, Compositi e Biomateriali, Via P. Gaifami 18, 95126 Catania, Italy

[#]CNR-IPCF Istituto per i Processi Chimico-Fisici, Viale F. Stagno d'Alcontres 37, 98158 Messina, Italy

Supporting Information

ABSTRACT: The potential of pyrene-1-sulfonate to act as an emitting anion for the development of ionic liquids is explored here. Amphiphilic trimethylpropylammonium hepta(isooctyl)octasilsesquioxane and conventional imidazolium, namely, 1-vinyl-3-hexyl-, 1-vinyl-3-decyl-, and 1-methyl-3-decyl-imidazolium, featuring moderate alkyl chain length substituents, have been chosen as countercations. The new species have been synthesized via simple metathesis reactions involving pyrene-1-sulfonate sodium salt and the appropriate halide cation precursors. Their thermal behavior has been investigated by thermogravimetric and differential scanning calorimetry at different scanning rates. According to this latter technique, only the trimethylpropylammonium hepta(isooctyl)octasilsesquioxane pyrenesulfonate adduct, displaying a reversible glass transition at −4.2 °C, may be classified as an ionic liquid. All pyrene-1-sulfonate imidazolium-based ion pairs are crystalline solids with the melting point just above 100 °C that produce very complex, nonreversible, and scanning rate-dependent thermograms, very likely arising from polymorphism phenomena. Such a behavior may be attributed to the pyrene-1-sulfonate polycyclic system, which in solution, as confirmed through spectroscopic characterization, displays a general attitude in promoting supramolecular structures via cation interactions. Emission lifetime measurements on the emitting fluorophore reveal that there are at least two different active species, whereas light scattering measurements show the presence of aggregates with hydrodynamic radii depending on the medium and adduct concentration. Tests aimed at investigating the potential of these novel pyrene-1-sulfonate salts in functionalization/exfoliation of graphite flakes are also reported here.

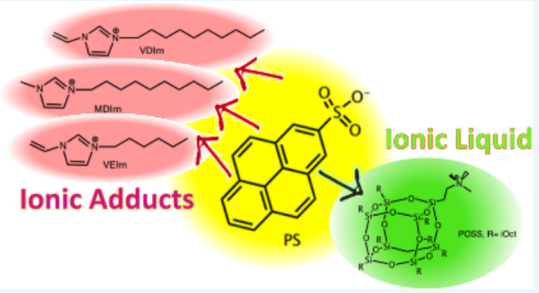

1. INTRODUCTION

Ionic liquids (ILs), defined as salts melting below 100 °C, have attracted extensive attention in the last 2 decades because of their custom-tailored physicochemical properties, such as low vapor pressure, wide liquid range, excellent chemical, thermal, and electrochemical stability, dispersant capabilities, dielectric constants, extraction capabilities, and so on.[1−3] As such, ILs are highly versatile media replacing conventional organic solvents and electrolytes, finding applications in many strategic fields such as catalysis, electrochemical devices, separation processes, synthesis, nanochemistry, photonics, and, more recently, biotechnology.[4−10] Anchoring of IL units to proper substrates such as polymer networks and/or nanomaterials is a successful synthetic methodology to access IL-based materials, usually referred to as supported ILs (SILs), with higher processing performance and even new functions.[11−17] Among others, by promoting ionic self-assembly processes, ILs and SILs have shown to be ideal precursors leading to advanced ionic supramolecular assemblies.[18−21]

ILs with intrinsic functions, usually defined as task-specific ILs, are easily obtained by introducing active ions in IL structures.[22−24] Thanks to the high disposal of organic emitter ions, this approach is a useful means to access novel soft photoluminescent materials, alternative to rare-earth fluorophores, for application in photonics, sensing, optoeletronic devices, dye-sensitized solar cells, and so on.[12,25−29] By using this strategy, ILs with improved physico-chemical properties and processing capabilities, such as solubility, photostability,

Received: October 26, 2018
Accepted: December 18, 2018
Published: December 28, 2018

Downloaded via Placido Mineo on December 29, 2018 at 19:25:34 (UTC).
See https://pubs.acs.org/sharingguidelines for options on how to legitimately share published articles.

© 2018 American Chemical Society

DOI: 10.1021/acsomega.8b02961
ACS Omega 2018, 3, 18811−18820

high quantum yields, and so on, differing significantly from those of the related salts, have been obtained.[30−35] Further, systematic studies also showed that the photoactivity of ILs constitutes, to some extent, a tunable, structurally controlled IL function.[36,37]

Because of the high relevance of the so-called "POSS nanotechnology" (POSS = polyhedral oligomeric silsesquioxanes) in the context of materials science, we have devoted our attention to the development of POSS-based ILs. Briefly, POSS are cage-like hybrid units with empirical formula $(SiO_{1.5})_x$ consisting of an inner inorganic core tethered with organic substituents widely used as efficient nanofillers inducing improved thermal, mechanical, and oxidation stability. Interestingly, when POSS is used as a scaffold for covalent binding of photoluminescent moieties, it experiences, among others, a dispersing action, which results in a significant improvement of quantum efficiency.[38−42] In the course of our studies on POSS tetraalkylammonium-based ILs,[38−40] we have reported on the synthesis and photochemical characterization of 1:4 POSS@TPPS ILs based on *meso*-tetrakis-(4-sulfonatephenyl)porphyrin tetraanion (TPPS) and the POSS monofunctionalized cation, trimethylpropylammonium hepta-(isooctyl)octasilsesquioxane.[41] The synthesis, based on a simple biphasic chloroform/water process, as well as the resulting optical properties, is highly dependent on the amphiphilic nature of the bulky cation. The latter acts as a highly dispersant agent in chlorinated solvents, reducing the well-known aggregation tendency of the TPPS tetra-anion, both in solution and in the solid state. Therefore, long emission lifetimes were observed for both the TPPS anions and TPPS J-aggregates. Analogous to porphyrins, pyrene derivatives constitute a class of attractive and thoroughly investigated solvatochromic fluorophores widely applied in optoelectronics, biochemistry, and sensor fields. These compounds are characterized by long excited-state lifetime and, in concentrated solution and in the solid state, lead to characteristic excimers because of self-association phenomena.[42−53] Furthermore, pyrene acts as a probe for the local environment polarity because the intensity ratio of the first to third vibronic emission bands (I/III ratio) is very sensitive to the solvent polarity.[48] On the basis of these considerations, pyrene sulfonate anions were chosen for the development of novel photoluminescent ILs.

In the present study, we report on the synthesis and characterization of a series of ion pairs based on monofunctionalized pyrene-1-sulfonate (PS). Because of their high versatility and applications, besides trimethylpropylammonium hepta(isooctyl)octasilsesquioxane, conventional imidazolium cations, featured by "moderately" long alkyl chains, have been also considered as PS counterions (Scheme 1). Vinyl-imidazolium-based ILs are commonly used and they find a plethora of applications in various fields. It is well known that their properties can be opportunely tuned by varying the alkyl chain length. In addition, we chose to use vinyl-imidazolium derivatives to achieve potentially cross-linkable systems, thus tuning the IL properties. Furthermore, it has been reported that the presence of a vinyl substituent on the imidazolium ring provides additional hydrogen bonding interactions between the cations and anions whose strength decreases with increasing anion size.[21] The new 1:1 ionic adducts were characterized by matrix-assisted laser desorption/ionization-time of flight (MALDI-TOF) mass spectrometry, thermogravimetric analysis (TGA), differential scanning calorimetry (DSC), and a series of spectroscopic techniques (NMR, UV−vis, steady-state, and time-resolved fluorescence spectroscopy). We anticipate that while the POSS−pyrene adduct is classifiable as an IL, the imidazolium ones, featuring melting points above 100 °C, have to be considered as simple ion pairs.

Scheme 1. Schematic Representation and Abbreviations of PS Adducts

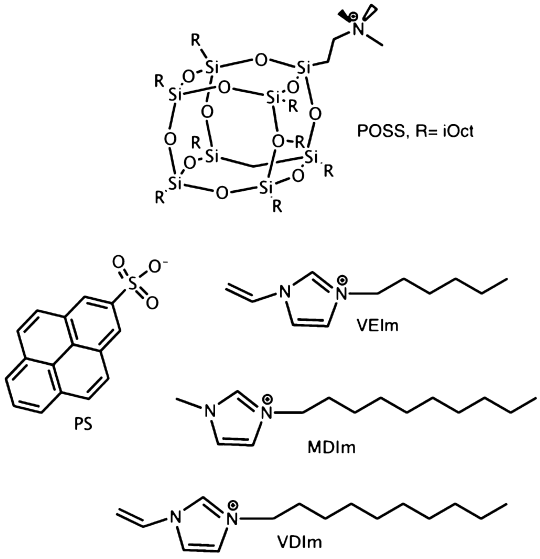

The combination of spectroscopic and light scattering data support the monomeric nature of the POSS−PS adducts in solution. On the contrary, imidazolium derivatives display a general attitude to self-organize in supramolecular structures through cation interactions, with the polycyclic anion acting as a nucleation center.

2. RESULTS AND DISCUSSION

2.1. Synthesis and Characterization. As described in the Experimental Section, PS POSS−ammonium and imidazolium derivatives (Scheme 1) were synthesized in high yields according to simple metathesis reactions. All new adducts have been obtained as pale yellow solids, except for POSS−PS, which appears very sticky, consistent with the nature of the cation. The characterization of the new ionic adducts was carried out by elemental analyses, conventional spectroscopic techniques (UV−vis, static and time-resolved fluorescence emission, and NMR spectroscopy), and MALDI−TOF spectrometry. Karl Fischer titrations reveal no significant level of water. Nevertheless, all samples were dried under vacuum overnight at 50 °C.

The ^{1}H NMR spectra of the new ionic adducts display a signal pattern consistent with the presence of an asymmetric pyrene group between δ 8−9.5 ppm, which well integrates 1:1 with those of the cation counterpart. The presence of the PS polycyclic anion does not produce other significant changes with respect to those of the parent IL halides: the only exception concerns the up-field shifts observed for the NC(H)N imidazolium protons that, as it is well known, are very sensitive to the nature of the anion. MALDI-TOF mass spectra of all new ion pairs (see Supporting Information) show the presence of a single signal corresponding to the molecular mass peak of the ionic species.

The thermal behavior of the new ionic PS adducts has been investigated by DSC and TGA analyses (Table 1). As reported

DOI: 10.1021/acsomega.8b02961
ACS Omega 2018, 3, 18811−18820

Table 1. Thermal Data of PS Adducts

	DSC heating					DSC cooling		TGA		
	T_g/°C	[a]T_{recrys}/°C	ΔH_{recrys} (J g^{-1})	T_{melt}/°C	ΔH_{melt} (J g^{-1})	T_{solid}/°C	ΔH_{solid} (J g^{-1})	T_{onset}/°C	[b]T_{max} (°C)	[c]residue/%
POSS−PS	−4.2							323.4	338.8, 465.2	4.3
VEIm−PS	22.2	42.7, 79.9	17.52, 7.39	124.5	−79.99	98.0	28.36	272.4	313.6	0.9
MDIm−PS		113.7	10.97	132.0	−62.58	114.0	55.06	308.7	395.1	0.9
VDIm−PS				120.9, 135.7	−26.75, −10.20	104.8	47.59	278.5	319.4	9.3

[a]T_{recrys}: temperature of recrystallization (T_{onset}). [b]T_{max}: temperature of the maximum rate of degradation. [c]Residue at 800 °C under N_2 flow at 10 °C min^{-1}.

in Table 1 and Figure 1, the occurrence of only a reversible glass transition at −4.2 °C and no melting point under 100 °C

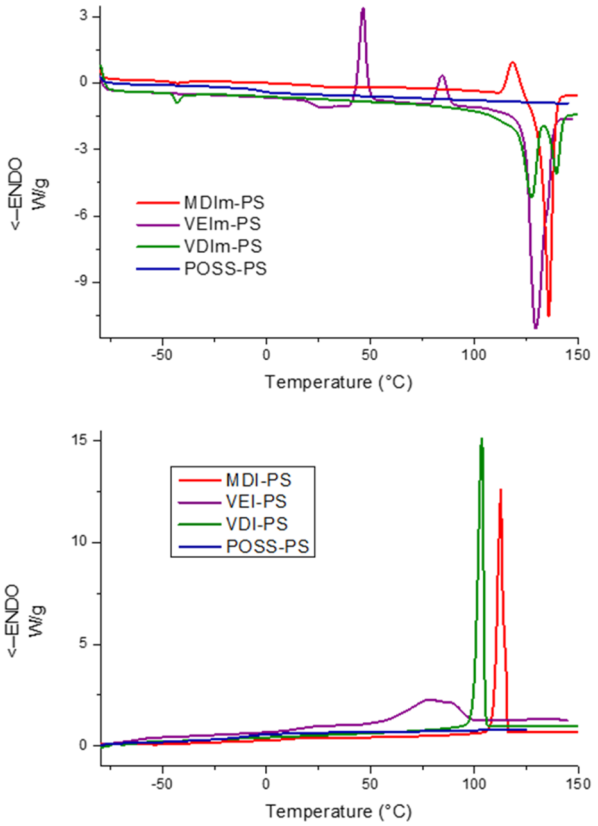

Figure 1. Heating (lower) and cooling DSC (upper) profiles at 10 °C min^{-1}.

(DSC data) indicate that POSS−PS may be defined as an IL. Accordingly, imidazolium−PS must be considered as simple ion pair couples.

With respect to POSS−PS, imidazolium derivatives afford more complex and diversified DSC responses. Figure 1 (upper) reports the heating course for all imidazolium samples, collected at 10 °C min^{-1}. The curve of 1-vinyl-3-hexylimidazolium (VEIm)−PS features a broad and weak endothermic event at 22.2 °C, followed by two distinct exothermic peaks at 42.7 and 79.9 °C, pointing to the occurrence of amorphous-to-crystal and solid-to-solid transitions, respectively, together with a broad endothermic event at 124.5 °C (T_{onset}). Actually, the shape of this last peak is not sharp, suggesting overlapped melting events. DSC thermograms of VDIm−PS present two very narrow endothermic events (120.9 and 135.7 °C), very likely associated with the melting of two distinct crystalline species with different arrangements or packing.

Finally, the DSC scan of 1-methyl-3-decylimidazolium (MDIm)−PS, bearing a methyl group in place of vinyl on the imidazolium ring, features a weak exothermic process (T_{onset} = 113.7 °C), immediately followed by a melting event at 132 °C. The observed heating transition phase profiles are not reversible. In the corresponding cooling curves (Figure 1, lower), only a liquid-to-solid process is observed for all the samples.

This exothermic process is well defined for both MDIm− and VDIm−PS (T_m = 114.0 and 104.8 °C, respectively), while for VEIm−PS, it shows unresolved multipeaks with T_{onset} at 98 °C. As expected, by lowering the DSC heating/cooling scan rate to 2 °C min^{-1} (see Supporting Information), different DSC thermograms have been obtained. In the heating scan, the melting transition for MDIm−PS is featured by two narrow peaks at 132.1 and 135.4 °C, very likely arising from two distinct crystal-to-liquid phase transitions. The melting process for VDIm−PS is detected as a broad signal with a T_{onset} of 133.43 °C and T_{max} of 138.0 °C, which is preceded by a solid-to-crystal transition. By cooling, an unresolved double exothermal peak is observed for MDIm−PS at 114.0 °C, while for VDIm−PS, a crystallization peak appears at 104.8 °C. Conversely, VEIm−PS affords a heating curve displaying an endothermal peak at 125.7 °C and a cooling one featuring a broad exo-multipeak with T_{onset} at 98.0 and T_{max} at 88.5 °C. The thermal behavior of imidazolium ILs/salts has been widely explored, and the role played by the nature of cations and/or anions, alkyl chain lengths on the aromatic ring, and intermolecular forces and symmetry in determining glass, melting, and meso- and polymorphic-phase transitions has been demonstrated.[21,54−56] On the basis of our experimental findings, it is reasonable to suppose that as solids, Imi−PS can be organized in supramolecular structures, via the alkyl chain, which can undergo "order−disorder" or vice versa phase transitions, thus affording nonreversible heating/cooling cycles and different DSC scanning profiles at different heating rates.[57] On the other hand, recent reports have described the role played by pyrene moieties in promoting and controlling the polymorphic superstructures of asymmetric dendritic biphenyl-based supramolecules.[57] Our DSC data suggest that (i) the thermal transition phase behavior of POSS−PS is still determined by the bulky amphiphilic nature of the trimethylpropylammonium hepta(isooctyl) octasilsesquioxane cation[39] and (ii) the substitution of bromide with a PS anion produces significant modifications on imidazolium-ILs, in terms of the melting point increase and the overall DSC thermogram profiles.[14,21] Although the DSC technique is currently used for the determination of thermodynamic parameters of ILs/salts, it is not able to give satisfactory information on molecular and supramolecular polymorphic

DOI: 10.1021/acsomega.8b02961
ACS Omega 2018, 3, 18811−18820

structures. Further investigation of the thermal behavior for these imidazolium−PS ionic adducts goes beyond the aim of the present study. The thermal stability of the new adducts was determined by TG analyses (Figure 2, Table 1) in the

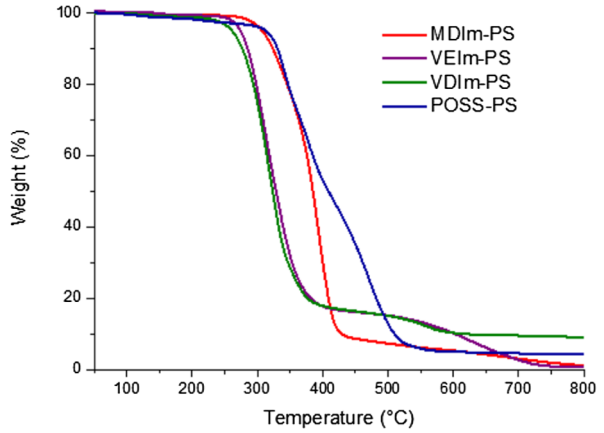

Figure 2. Thermogravimetric traces of MDIm−PS, VEIm−PS, VDIm−PS, and POSS−PS.

temperature range between 50 and 800 °C, under a nitrogen flow (60 mL min^{-1}) and heating rate of 10 °C min^{-1}. The TGA profile of POSS−PS proceeds, essentially, in a large temperature range for which two temperatures of maximum volatilization (338.8 and 465.2 °C) are observed. The imidazolium−PS adducts afford very similar thermograms, as the mass losses take place in a single step. As their thermal stability is concerned, TGA data suggest that the presence of the vinyl substituent on the imidazolium ring induces a lower stability. Accordingly, VDIm−PS displays T_{onset} and T_{max} values significantly lower than those observed for MDIm−PS.

2.2. Photophysical Behavior in Solution. All the samples displayed a similar behavior in terms of good solubility in solvents with different polarities [tetrahydrofuran (THF), $CHCl_3$, and MeOH] up to millimolar concentration, where they are stable for months, as confirmed by the invariance of the UV−vis and fluorescence emission spectra. The photophysical properties and aggregation behavior of these adducts have been investigated in chloroform and methanol solution by various spectroscopic and light scattering techniques. Pyrene-1-sulfonate−tetra-*n*-butyl ammonium salt (TBA−PS) has been used as a reference. The UV−vis and fluorescence emission spectra in chloroform and methanol are similar for all the investigated samples. As an example, Figure 3 reports the spectroscopic features of MDIm−PS. Absorption bands with a characteristic vibronic fine structure, between 300 and 350 nm (upper graph), together with a structured emission band centered at ca. 378 nm (lower graph) are typical of the pyrene chromophore. The observed ipsochromic shift of the absorption bands in methanol with respect to chloroform ($\Delta\lambda$ = −3 nm), together with intensity ratio modulation of the first to third vibronic emission bands, is ascribable to the change in solvent polarity. Beer's law is obeyed up to millimolar concentrations and no additional nonstructured band at longer wavelengths, characteristic of excimer emission, has been observed for all the species.[58] To confirm the absence of the excimer in solution, emission spectra at different sample concentrations and excitation spectra at different emission wavelengths have been collected (see Supporting Information). In any case, no evidence for the presence of excimers has been

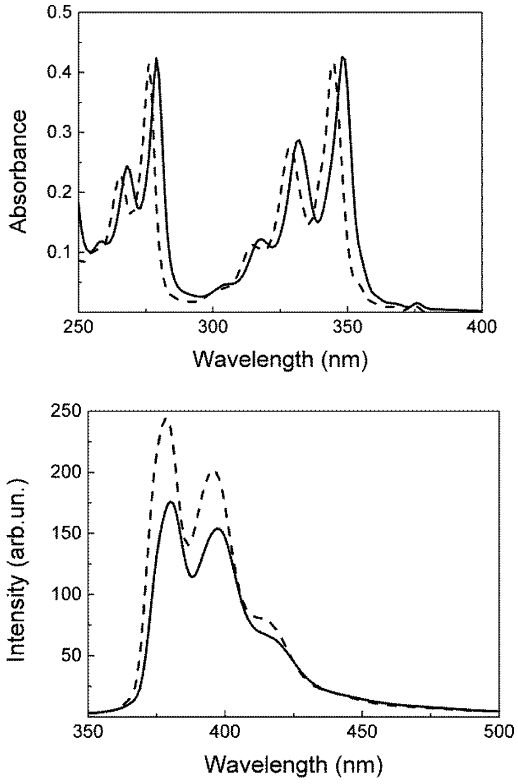

Figure 3. Absorption (upper) and fluorescence emission (lower) spectra of MDIm−PS in chloroform (solid line) and methanol (dashed line) solution. [MDIm−PS] = 13 μM, λ_{ex} = 340 nm.

obtained. The fluorescence emission decays, in aerated solutions, show a biexponential profile with comparable long-lifetime values from 4.6 to 4.8 ns and a short one from 1.4 for MDIm to 2.1 ns ca. for POSS. As an example, Figure 4 shows a typical decay trace, while lifetimes and relative amplitude values are shown in Table 2.

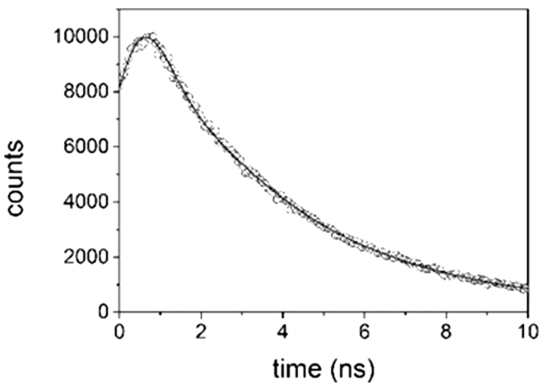

Figure 4. Time-resolved fluorescence decay of VDIm−PS in chloroform. [VDIm−PS] = 10 μM, T = 298 K, λ_{ex} = 390 nm, λ_{em} = 450 nm.

The two emission lifetime values are consistently shorter than those reported for PS sodium salt (PS−Na) in aqueous solution but very similar to those obtained for TBA−PS in apolar solvent. This experimental evidence underlines that the presence of oxygen could be responsible for this discrepancy. The biexponential decay curves observed for these PS adducts are clearly indicative of two different species in solution.

DOI: 10.1021/acsomega.8b02961
ACS Omega 2018, 3, 18811−18820

Table 2. Fluorescence Lifetimes (τ/ns), Relative Amplitude (A/%), and Rotational Correlation Time [$r(t)$/ns] for PS–Imidazolium Derivatives in $CHCl_3$[a]

sample	τ_1/ns	τ_2/ns	A_1	A_2	$r(t)$/ns
[b]PS–Na	3.2 ± 0.02	54.2 ± 0.3	10	90	
TBA–PS	1.7 ± 0.04	4.6 ± 0.02	40	60	1.04 ± 0.03
MDIm–PS	1.4 ± 0.05	4.7 ± 0.02	32	68	0.97 ± 0.05
VDIm–PS	1.6 ± 0.05	4.6 ± 0.02	35	65	1.02 ± 0.05
VEIm–PS	1.8 ± 0.05	4.7 ± 0.02	32	68	1.01 ± 0.08
POSS–PS	2.1 + 0.03	4.8 + 0.01	43	57	1.05 ± 0.05
GF/VDIm–PS	1.6 ± 0.03	3.7 ± 0.04	14	86	

[a]10 μM, T = 298 K, λ_{ex} = 390 nm, λ_{em} = 450 nm. [b]H_2O.

The fluorescence anisotropy decay [$r(t)$], which allows us to gain information on the formation of supramolecular structures via the rotational diffusion of the fluorophores, gives a rotational correlation time of about 1 ns, which is not fully compatible with the size of the single molecule (see data in Table 2). Further, the rotational correlation time suggests that the free rotation of each single fluorophore is partially inhibited.

In order to investigate the aggregation behavior in solution, dynamic light scattering (DLS) experiments were performed at different concentrations of PS–imidazolium derivatives in chloroform and methanol solutions. DLS data collected in Table 3 are in line with the presence in solution of a monodisperse population of spheric aggregates with hydrodynamic radii R_H depending on the solvent polarity and adduct concentration. In chloroform, only some aggregate structures are detectable at low concentrations (1 μM), while larger ones are well identifiable at highest concentrations (100 μM). In the more polar methanol, nanometer-sized aggregates are already detectable at very low concentrations (1 μM). This behavior could be ascribed to assembling phenomena involving imidazolium cations. Comparative DLS experiments, performed on MDIm, VDIm, and VEIm bromide precursors, indicate that these compounds have no tendency to self-aggregate, independent of the alkyl chain length on the imidazolium ring. The absence of resonant light scattering peaks in the PS absorption region (see Supporting Information) allows us to exclude the presence of extended PS aggregates resulting from the strong electronic coupling of adjacent chromophores. However, it does not exclude the formation of dimer or small oligomers, which could be responsible for the observed spectroscopic behavior. Hence, on the basis of these DLS and photophysical investigations, we can speculate on the formation of supramolecular species obtained by the interaction between PS anion as monomers, dimers, or small oligomers embedded in nanostructured aggregates, mainly because of countercation supramolecular self-assembly with a consequent consistent reduction of the fluorophore mobility. We can conclude that extended stacking is not observed, presumably owing to the great "edge" effect due to the alkyl chains of countercations.

Table 3. Hydrodynamic Radii for PS–Imidazolium Derivatives in $CHCl_3$ and MeOH at Different Adduct Concentrations

	R_H/nm in $CHCl_3$		
	1 μM	10 μM	100 μM
MDIm–PS		25 + 4	100 + 11
VDIm–PS		25 + 3	50 + 7
VEIm–PS		33 + 8	70 + 10
	R_H/nm in MeOH		
	1 μM	10 μM	100 μM
MDIm–PS	80 + 20	95 + 18	150 + 36
VDIm–PS	50 + 7	50 + 10	100 + 22
VEIm–PS	25 + 4	50 + 12	100 + 25

2.3. Interaction of PS Adducts with Graphite Flakes.

Polycyclic aromatic compounds, based on pyrene, perylene, and so forth, in a simple ionic or amphiphilic properly functionalized form constitute useful species for a supramolecular approach in graphite (GR) exfoliation to graphene as well as for noncovalent modification of graphitic surfaces.[59−61] Among others, various substituted pyrene salts have been successfully employed in shear-assisted exfoliation of natural GR as well as of GR flakes (GFs).[62,63] On the other hand, thanks to their ionic nature and their tunable surface

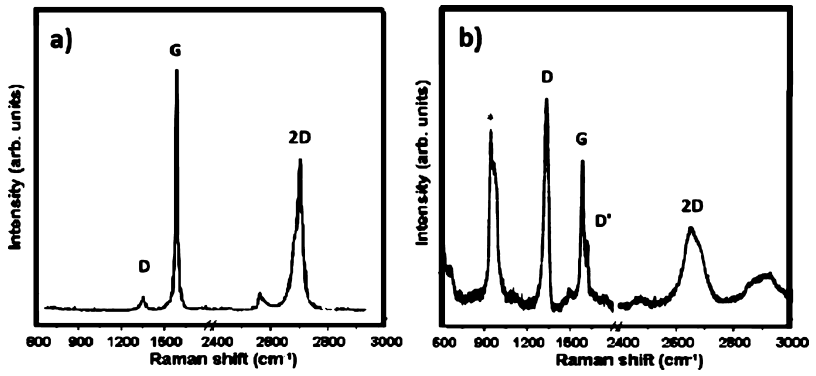

Figure 5. Raman spectra of (a) GFs and (b) GFs@VDIm–PS. (*) Peaks assigned to the PS moiety.

DOI: 10.1021/acsomega.8b02961
ACS Omega 2018, 3, 18811−18820

tension, ILs are an ideal "solvent" for GR exfoliation and stabilization of graphene suspensions.[64−66]

Stable GFs/PS-adduct THF suspensions have been obtained by using a sonication-assisted liquid phase procedure as described in the Experimental Section. These suspensions have been analyzed by UV−vis and Raman spectroscopy, the latter being one of the most powerful tools to investigate graphitic surfaces and edge modifications. All the GFs@PS-adduct composites afford comparable electronic and Raman spectra; hence, the discussion will be limited to the GFs@VDIM−PS sample.

According to Figure 5a, the Raman spectrum of GFs is consistent with a graphitic system bearing no significant structural defects, featuring a disordered, related low-intensity D peak at 1352 cm^{-1}, a sharp G band at 1578 cm^{-1}, ascribed to E_{2g} vibrational mode, and the 2D one centered at around 2718 cm^{-1} and characterized by two subbands, namely, $2D_2$ and $2D_1$.[67]

In the GFs/VDIM−PS Raman spectrum (Figure 5b), the GF pre-existing bands show a different intensity ratio, while new ones appear. In particular, the D band intensity increases, the G band is slightly split at a higher wavenumber, and the contribution D′ is now detectable at 1621 cm^{-1}. At the same time, the 2D pattern is broader and shifted to lower energy with the $2D_1$ component (at around 2690 cm^{-1}) more pronounced.[68] The intense band in the range 900−1050 cm^{-1} is attributable to the PS moiety.[69]

The UV−vis absorption spectra of VDIm−PS and GFs@VDIM−PS in THF solution are reported in Figure 6. By comparison, the modification induced by the presence of GFs on the VDIm−PS pattern is clearly evident. Even the fluorescence emission properties are modified (Table 3). The emission decay of GFs@VDIM−PS shows a biexponential profile with lifetimes of 3.7 and 1.6 ns and with relative amplitudes of 86 and 14%, respectively. The longest lifetime is shorter with respect to that of the VDIm−PS precursor (4.6 ns), while the relative amplitude is largely increased.

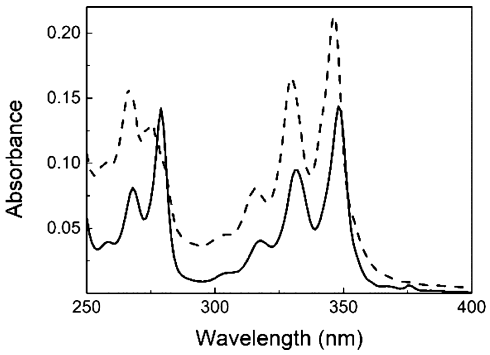

Figure 6. Absorption spectra of VDIm−PS in THF (solid line) and GFs@VDIm−PS (dashed line) in THF.

Even if the supramolecular interactions between the PS anion and GFs occur, they are not sufficient to afford an efficient exfoliation to graphene. For the sake of comparison, we have also explored the capabilities of halide IL precursors in GF processing. As an example, imidazolium bromide in THF solutions produces significant exfoliation of GFs, [see Raman and scanning transmission electron microscopy (STEM) analyses in Supporting Information]. This finding suggests that the PS polycyclic system is responsible for noncovalent functionalization of the GF surface and that the nature of cations does not play any synergic role in the GR exfoliation process.

3. CONCLUSIONS

As part of our general interest regarding the design and synthesis of functional and SILs, here, we have reported on the PS anion attitude in generating fluorescent ILs. Amphiphilic trimethylpropylammoniumhepta(isooctyl)-octasilsesquioxane and conventional imidazolium have been chosen as counter-cations. The experimental evidence shows that among the series of synthesized PS ion pairs, only the POSS derivative exhibits an IL behavior. Different from IL halide precursors, all imidazolium−PS derivatives display a crystalline nature. The PS anion, which does not undergo self-assembly processes, seems to play a main role in promoting the formation of imidazolium polymorphic structures, which are responsible for their complex transition phases. DLS investigations confirm the presence in solution of nanometer-sized species whose dimension is dependent on the solvent polarity and sample concentration; meanwhile, spectroscopic data indicate the absence of the extended electronically coupled chromophores in these supramolecular aggregates. These findings suggest, once more, that the presence of bulky surfactant cations is demanding in the design of luminescent-based PS ILs and more in general of ILs involving highly delocalized anions. Finally, we have also explored the capabilities of the new compounds in GF processing. On the basis of Raman data, we suggest that simple supramolecular interactions are operating between the PS anion and GF surface. These noncovalent forces are responsible for the stabilization observed in THF dispersion.

4. EXPERIMENTAL SECTION

4.1. Materials and Methods. All the chemicals and solvents employed, unless otherwise stated, were purchased from Sigma-Aldrich; aminopropylisobutyl POSS and aminopropylisooctyl POSS were purchased from Hybrid Plastics; all these compounds were used as received. 1-Methyl-3-hexylimidazolium bromide, VEIm bromide, MDIm bromide, and 1-vinyl-3-decylimidazolium bromide were obtained according to a published procedure.[14] Trimethylpropylammonium hepta(isobutyl) octasilsesquioxane iodide and trimethylpropylammonium hepta(isooctyl) octasilsesquioxane iodide were synthesized following a protocol already reported.[39]

4.2. Synthesis. *4.2.1. Trimethylpropylammonium hepta(isooctyl)octasilsesquioxane Pyrene-sulfonate (**POSS−PS**).* A suspension of 1-pyrenesulfonic acid sodium salt (0.1 g, 0.33 mmol) in 20 mL of deionized water was added dropwise to 0.430 g of trimethylpropylammoniumhepta(isooctyl) octasilsesquioxane iodide (0.30 mmol) dispersed in 10 mL of deionized water. The reaction mixture was left at 75 °C under vigorous stirring for 72 h. After decantation, the product separated as a sticky yellow solid; it was washed three times with water and then dried in a Rotavapor at 80 °C. Yield: 62%. ^{1}H NMR ($CDCl_3$, δ, ppm): 0.66 (br, 16H), 0.87 (m, 65H), 0.99 (d, 21H), 1.81 (br, 9H), 3.31 (m, 2H), 3.38 (s, 9H), 8.21−8.00 (m, 7H), 8.73 (d, 1H), 9.35 (d, 1H). ^{29}Si{^{1}H} NMR ($CDCl_3$, δ, ppm): −67.34, −68.05, −69.04, −70.78. Elemental analysis: Calcd for $C_{78}H_{143}NO_{15}SSi_8$ (1591.75): C, 58.86%; H, 9.06%; N, 0.88%. Found: C, 58.87%; H, 9.09%; N,

DOI: 10.1021/acsomega.8b02961
ACS Omega 2018, 3, 18811−18820

0.91%. MALDI-TOF (m/z): 1591.3 (detected at m/z 2900.5 as $[M]^{POSS+}$ adduct).

4.2.2. 1-Vinyl-3-hexylimidazolium PS. **VEIm−PS** was obtained as a pale yellow solid using the same synthetic protocol as for **MEIm−PS**, by reacting 0.25 g (0.82 mmol) of 1-pyrenesulfonic acid sodium salt and 0.78 g of **VEIm** bromide (0.68 mmol) in deionized water. Yield: 69%. ^{1}H NMR ($CDCl_3$, δ, ppm): 0.71 (m, 3H), 1.01 (m, 6H), 1.58 (m, 2H), 4.05 (m, 2H), 5.17 (m, 1H), 5.70 (m, 1H), 7.11 (m, 1H), 7.22 (m, 1H), 7.42 (m, 1H), 8.20−7.99 (m, 7H), 8.72 (d, 1H), 9.31 (d, 1H), 10.25 (s, 1H). Elemental analysis: Calcd for $C_{27}H_{28}N_2O_3S$ (460.59): C, 70.41%; H, 6.13%; N, 6.08%. Found: C, 70.56%; H, 6.12%; N, 6.06%. UV−vis ($CHCl_3$): ($\lambda_{max/nm}$) 348 ($\varepsilon = 3.89 \times 10^4$ M^{-1} cm^{-1}), 258, 268, 278, 317; 331. Fluorescence emission ($CHCl_3$): ($\lambda_{exc/nm}$) 340, ($\lambda_{em/nm}$) 378, 397,417. MALDI-TOF (m/z): 460.8 (detected at m/z 639.2 as $[M]^{VEIm+}$ adduct).

4.2.3. 1-Methyl-3-decylimidazolium PS. **MDIm−PS** was obtained as a waxy pale yellow solid employing a procedure similar to that for **MEIm−PS**, using 0.32 g (1.05 mmol) of 1-pyrenesulfonic acid sodium salt in 20 mL of deionized water and 0.32 g of **MDIm** bromide (0.88 mmol). Yield: 76%. ^{1}H NMR ($CDCl_3$, δ, ppm): 0.86 (m, 3H), 1.16 (m, 14H), 1.65 (m, 2H), 3.98 (s, 3H), 4.03 (m, 2H), 7.01 (m, 1H), 7.11 (m, 1H), 8.21−7.97 (m, 7H), 8.75 (d, 1H), 9.34 (d, 1H), 9.94 (s, 1H). Elemental analysis: Calcd for $C_{30}H_{36}N_2O_3S$ (504.68): C, 71.40%; H, 7.19%; N, 5.55%. Found: C, 71.51%; H, 7.30%; N, 5.62%. UV−vis ($CHCl_3$): ($\lambda_{max/nm}$) 348 ($\varepsilon = 3.31 \times 10^4$ M^{-1} cm^{-1}), 258, 268, 278, 317; 331. Fluorescence emission ($CHCl_3$): ($\lambda_{exc/nm}$) 340, ($\lambda_{em/nm}$) 378, 397,417. MALDI-TOF (m/z): 505.0 (detected at m/z 727.4 as $[M]^{MDIm+}$ adduct).

*4.2.4. 1-Vinyl-3-decylimidazolium PS (**VDIm−PS**).* **VDIm−PS** was isolated as a waxy pale yellow solid following a synthetic procedure similar to the previous one, using 0.19 g (0.64 mmol) of 1-pyrenesulfonic acid sodium salt in 15 mL of deionized water and 0.0.17 g of 1-vinyl-3-decylimidazolium bromide (0.53 mmol). Yield: 72%. ^{1}H NMR ($CDCl_3$, δ, ppm): 0.85 (m, 3H), 1.17 (m, 14H), 1.57 (m, 2H), 4.05 (m, 2H), 5.47 (m, 1H), 5.66 (m, 1H), 7.12 (m, 1H), 7.22 (m, 1H), 7.43 (m, 1H), 8.16−7.99 (m, 7H), 8.72 (d, 1H), 9.30 (d, 1H), 10.23 (s, 1H). Elemental analysis: Calcd for $C_{31}H_{36}N_2O_3S$ (516.69): C, 72.06%; H, 7.02%; N, 5.42%. Found: C, 71.97%; H, 7.03%; N, 5.39%. UV−vis ($CHCl_3$): ($\lambda_{max/nm}$) 348 ($\varepsilon = 2.36 \times 10^4$ M^{-1} cm^{-1}), 258, 268, 278, 317; 331. Fluorescence emission ($CHCl_3$): ($\lambda_{exc/nm}$) 340, ($\lambda_{em/nm}$) 378, 397, 417. MALDI-TOF (m/z): 516.9 (detected at m/z 752.1 as $[M]^{MDIm+}$ adduct).

4.2.5. Exfoliation/Functionalization of GFs. In a general procedure, GFs (15 mg) and PS-based ionic adducts (30 mg) were grinded together in a mortar and then transferred into a vessel containing 15 mL of THF. The resulting mixture was sonicated for 24 h at room temperature then left to stand for 12 h, and finally centrifuged at 1300 rpm for 30 min to precipitate excess GF powder. The obtained light gray supernatant suspension has been used for analysis. By following a similar procedure, a specimen based on GFs and VDIm−Br was prepared for comparison.

4.3. Instruments. ^{1}H and ^{29}Si{^{1}H} NMR solution spectra were obtained in deuterated solvents at room temperature on a Bruker AMX R-300 spectrometer operating at 300.13 and 59.62 MHz for ^{1}H and ^{29}Si nuclei, respectively. Chemical shifts (δ, ppm) were referred to $SiMe_4$. TGA were performed by means of PerkinElmer Pyris TGA7 in the temperature range between 50 and 800 °C, under a nitrogen flow (60 mL min^{-1}) and heating rate of 10 °C min^{-1}. DSC measurements were carried out by using a TA Q20 instrument equipped with a refrigerant cooling system with a heating rate of 2 and 10 °C min^{-1}, in the −80 to +140 °C temperature range and under an anhydrous N_2 atmosphere (60 mL min^{-1}). MALDI-TOF mass spectra were acquired using Voyager DE (PerSeptive Biosystems) using an acquisition protocol reported elsewhere.[70−72] *trans*-2-[3-(4-*tert*-butylphenyl)-2-methyl-2-propenylidene]-malonitrile (DCTB) was used as the matrix. MALDI-TOF mass spectrometer calibration and average molecular mass determination were performed as reported in previous cases.[73,74] Because of the isotopic composition, molecular species are detected in the mass spectra as clusters of peaks; to simplify their assignments, m/z values reported in the text are referred to the first peak of each cluster, corresponding to the ion containing the most abundant isotope of each element present. Micro-Raman spectra have been excited by the 532 nm diode laser wavelength, analyzed by a monochromator equipped with a 1800 line/mm grating, and collected by a Peltier-cooled charge-coupled device (CCD) sensor. STEM observations were carried out with a Zeiss-Gemini 2 electron microscope, operating at an accelerating voltage of 150 kV and equipped with a MultiScan CCD camera. STEM samples are prepared by depositing one drop of the solution on a 400 μm meshe carbon support sputter-coated with chromium and left to dry at room temperature for 3 h. UV−vis spectra were obtained using a Hewlett-Packard mod. 8453 diode array spectrophotometer. Static and time-resolved fluorescence emission measurements were performed on a Jobin Yvon-Spex FluoroMax 4 spectrofluorimeter using the time-correlated single-photon counting technique. A NanoLED (λ = 390 nm) has been used as the excitation source. Emission spectra were not corrected for the absorbance of the samples. Resonance light scattering (RLS) experiments were performed on a Jasco mod. FP-750 spectrofluorimeter, adopting a synchronous scan protocol with a right angle geometry.[75] RLS spectra were not corrected for the inner-filter effect of the samples. Hydrodynamic particle sizes and size distributions were measured by DLS and carried out at 25 °C by a Zetasizer Nano-ZS (Malvern Instruments) equipped with a 633 nm He−Ne laser using backscattering detection. Each DLS sample was measured several times, and the results were averaged. IL stock solutions, obtained by dissolving the adducts in $CHCl_3$ and/or MeOH, were stored in the dark and used within a week from preparation. The range of concentration (1×10^{-6} to 5×10^{-4} M) used in our experiments was determined spectrophotometrically by using the molar extinction coefficient at the Soret maximum.

■ ASSOCIATED CONTENT

Supporting Information

The Supporting Information is available free of charge on the ACS Publications website at DOI: 10.1021/acsomega.8b02961.

Positive MALDI spectra of POSS−PS, VDI−PS, VEIm−PS, and MDIm−PS; DSC curves of MDIm−PS, VDIm−PS, and VEIm−PS; fluorescence emission, extinction, and RLS spectra of VDIm−PS; and Raman spectrum and STEM image of GFs@VDIm−Br (PDF)

DOI: 10.1021/acsomega.8b02961
ACS Omega 2018, 3, 18811−18820

AUTHOR INFORMATION

Corresponding Authors

*E-mail: castriciano@pa.ismn.cnr.it. Phone: +39 090 3974108 (M.A.C.).
*E-mail: sloschiavo@unime.it (S.L.S.).

ORCID

Maria Angela Castriciano: 0000-0002-1514-8820
Paola Cardiano: 0000-0002-1380-5380
Placido Giuseppe Mineo: 0000-0003-3382-9272
Luigi Monsù Scolaro: 0000-0002-9742-9190

Author Contributions

The manuscript was written through contributions of all authors. All authors have given approval to the final version of the manuscript.

Notes

The authors declare no competing financial interest.

ACKNOWLEDGMENTS

The authors thank CNR for financial support "Nanomateriali e nanotecnologie per lo sviluppo sostenibile ed il patrimonio culturale" (CUP: G78B14000100006, 1/2012, grant to R.Z.) and MatISSE" Materiali Innovativi e Sostenibili per la Salute e l'Energia (CUP G77B17000180009, grant to M.T.)

REFERENCES

(1) Armand, M.; Endres, F.; MacFarlane, D. R.; Ohno, H.; Scrosati, B. Ionic-Liquid Materials for the Electrochemical Challenges of the Future. *Nat. Mater.* **2009**, *8*, 621−629.
(2) Greaves, T. L.; Drummond, C. J. Protic Ionic Liquids: Properties and Applications. *Chem. Rev.* **2008**, *108*, 206−237.
(3) MacFarlane, D. R.; Pringle, J. M.; Howlett, P. C.; Forsyth, M. Ionic Liquids and Reactions at the Electrochemical Interface. *Phys. Chem. Chem. Phys.* **2010**, *12*, 1659−1669.
(4) De Leo, F.; Cardiano, P.; De Carlo, G.; Lo Schiavo, S.; Urzì, C. Testing the antimicrobial properties of an upcoming "environmental-friendly" family of ionic liquids. *J. Mol. Liq.* **2017**, *248*, 81−85.
(5) Egorova, K. S.; Gordeev, E. G.; Ananikov, V. P. Biological Activity of Ionic Liquids and Their Application in Pharmaceutics and Medicine. *Chem. Rev.* **2017**, *117*, 7132−7189.
(6) Plechkova, N. V.; Seddon, K. R. Applications of Ionic Liquids in the Chemical Industry. *Chem. Soc. Rev.* **2008**, *37*, 123−150.
(7) Seddon, K. R. A Taste of the Future. *Nat. Mater.* **2003**, *2*, 363−365.
(8) Shamshina, J. L.; Kelley, S. P.; Gurau, G.; Rogers, R. D. Chemistry: Develop Ionic Liquid Drugs. *Nature* **2015**, *528*, 188−189.
(9) Sivapragasam, M.; Moniruzzaman, M.; Goto, M. Recent Advances in Exploiting Ionic Liquids for Biomolecules: Solubility, Stability and Applications. *Biotechnol. J.* **2016**, *11*, 1000−1013.
(10) Torimoto, T.; Tsuda, T.; Okazaki, K.-i.; Kuwabata, S. New Frontiers in Materials Science Opened by Ionic Liquids. *Adv. Mater.* **2010**, *22*, 1196−1221.
(11) Cardiano, P.; Gómez-Laserna, O.; Mineo, P. G.; Furia, E.; Triolo, C.; Patanè, S.; Lo Schiavo, S. Synthesis, Co2 Sorption and Capacitive Properties of Novel Protic Poly(Ionic Liquid)S. *J. Mol. Liq.* **2017**, *241*, 222−230.
(12) Le Bideau, J.; Viau, L.; Vioux, A. Ionogels, ionic liquid based hybrid materials. *Chem. Soc. Rev.* **2011**, *40*, 907−925.
(13) Mineo, P. G.; Livoti, L.; Giannetto, M.; Gulino, A.; Lo Schiavo, S.; Cardiano, P. Very Fast Co2 Response and Hydrophobic Properties of Novel Poly(Ionic Liquid)S. *J. Mater. Chem.* **2009**, *19*, 8861−8870.
(14) Mineo, P. G.; Livoti, L.; Lo Schiavo, S.; Cardiano, P. Fast and reversible CO2quartz crystal microbalance response of vinylimidazolium-based poly(ionic liquid)s. *Polym. Adv. Technol.* **2011**, *23*, 1511−1519.
(15) Patanè, S.; Triolo, C.; Cardiano, P.; Lo Schiavo, S. Capacitive Properties of the Hydrophobic [2-(Methacryloyloxy)Ethyl]-Trimethyl Ammonium Nonafluoro-1-Butanesulfonate Poly(Ionic Liquid) Thin Film. *Ionics* **2017**, *23*, 1481−1487.
(16) Qian, W.; Texter, J.; Yan, F. Frontiers in Poly(Ionic Liquid)S: Syntheses and Applications. *Chem. Soc. Rev.* **2017**, *46*, 1124−1159.
(17) Yuan, J.; Mecerreyes, D.; Antonietti, M. Poly(Ionic Liquid)S: An Update. *Prog. Polym. Sci.* **2013**, *38*, 1009−1036.
(18) Ali Aboudzadeh, M.; Eugenia Muñoz, M.; Santamaría, A.; Marcilla, R.; Mecerreyes, D. Facile Synthesis of Supramolecular Ionic Polymers That Combine Unique Rheological, Ionic Conductivity, and Self-Healing Properties. *Macromol. Rapid Commun.* **2012**, *33*, 314−318.
(19) Blesic, M.; Marques, M. H.; Plechkova, N. V.; Seddon, K. R.; Rebelo, L. P. N.; Lopes, A. Self-Aggregation of Ionic Liquids: Micelle Formation in Aqueous Solution. *Green Chem.* **2007**, *9*, 481−490.
(20) Craig, S. L. From Ionic Liquids to Supramolecular Polymers. *Angew. Chem., Int. Ed.* **2009**, *48*, 2645−2647.
(21) Luo, S.-C.; Sun, S.; Deorukhkar, A. R.; Lu, J.-T.; Bhattacharyya, A.; Lin, I. J. B. Ionic Liquids and Ionic Liquid Crystals of Vinyl Functionalized Imidazolium Salts. *J. Mater. Chem.* **2011**, *21*, 1866−1873.
(22) Cardiano, P.; Foti, C.; Mineo, P. G.; Galletta, M.; Risitano, F.; Lo Schiavo, S. Sequestration Ability of Task Specific Ionic Liquids Towards Cations of Environmental Interest. *J. Mol. Liq.* **2016**, *223*, 174−181.
(23) Giernoth, R. Task-Specific Ionic Liquids. *Angew. Chem., Int. Ed.* **2010**, *49*, 2834−2839.
(24) Han, X.; Armstrong, D. W. Ionic Liquids in Separations. *Acc. Chem. Res.* **2007**, *40*, 1079−1086.
(25) Imahori, H.; Umeyama, T.; Ito, S. Large π-Aromatic Molecules as Potential Sensitizers for Highly Efficient Dye-Sensitized Solar Cells. *Acc. Chem. Res.* **2009**, *42*, 1809−1818.
(26) Imahori, H.; Umeyama, T.; Kurotobi, K.; Takano, Y. Self-Assembling Porphyrins and Phthalocyanines for Photoinduced Charge Separation and Charge Transport. *Chem. Commun.* **2012**, *48*, 4032−4045.
(27) Kawano, R.; Katakabe, T.; Shimosawa, H.; Khaja Nazeeruddin, M.; Grätzel, M.; Matsui, H.; Kitamura, T.; Tanabe, N.; Watanabe, M. Solid-State Dye-Sensitized Solar Cells Using Polymerized Ionic Liquid Electrolyte with Platinum-Free Counter Electrode. *Phys. Chem. Chem. Phys.* **2010**, *12*, 1916−1921.
(28) Victoria Martínez-Díaz, M.; de la Torre, G.; Torres, T. Lighting Porphyrins and Phthalocyanines for Molecular Photovoltaics. *Chem. Commun.* **2010**, *46*, 7090−7108.
(29) Radivojevic, I.; Varotto, A.; Farley, C.; Drain, C. M. Commercially Viable Porphyrinoid Dyes for Solar Cells. *Energy Environ. Sci.* **2010**, *3*, 1897−1909.
(30) Armel, V.; Pringle, J. M.; Forsyth, M.; MacFarlane, D. R.; Officer, D. L.; Wagner, P. Ionic Liquid Electrolyte Porphyrin Dye Sensitised Solar Cells. *Chem. Commun.* **2010**, *46*, 3146−3148.
(31) Fan, B.; Wei, J.; Ma, X.; Bu, X.; Xing, N.; Pan, Y.; Zheng, L.; Guan, W. Synthesis of Lanthanide-Based Room Temperature Ionic Liquids with Strong Luminescence and Selective Sensing of Fe(III) over Mixed Metal Ions. *Ind. Eng. Chem. Res.* **2016**, *55*, 2267−2271.
(32) Fiorani, G.; Selva, M.; Perosa, A.; Benedetti, A.; Enrichi, F.; Licence, P.; Easun, T. L. Luminescent Dansyl-Based Ionic Liquids from Amino Acids and Methylcarbonate Onium Salt Precursors: Synthesis and Photobehaviour. *Green Chem.* **2015**, *17*, 538−550.
(33) Gago, S.; Cabrita, L.; Carlos Lima, J.; Branco, L. C.; Pina, F. Synthesis and Characterization of Luminescent Room Temperature Ionic Liquids Based on Ru(Bpy)(Cn)42−. *Dalton Trans.* **2013**, *42*, 6213−6218.
(34) Mallick, B.; Balke, B.; Felser, C.; Mudring, A.-V. Dysprosium Room-Temperature Ionic Liquids with Strong Luminescence and Response to Magnetic Fields. *Angew. Chem., Int. Ed.* **2008**, *47*, 7635−7638.
(35) Xu, H.-J.; Gros, C. P.; Brandès, S.; Ge, P.-Y.; Girault, H. H.; Barbe, J.-M. Room Temperature Ionic Liquids Based on Cationic

DOI: 10.1021/acsomega.8b02961
ACS Omega 2018, 3, 18811−18820

Porphyrin Derivatives and Tetrakis(Pentafluorophenyl)Borate Anion. *J. Porphyrins Phthalocyanines* **2011**, *15*, 560−574.
(36) Campbell, P. S.; Yang, M.; Pitz, D.; Cybinska, J.; Mudring, A.-V. Highly Luminescent and Color-Tunable Salicylate Ionic Liquids. *Chem.—Eur. J.* **2014**, *20*, 4704−4712.
(37) Wang, M.-Y.; Ma, R.; He, L.-N. Polyoxometalate-Based Ionic Liquids-Promoted Co2 Conversion. *Sci. China: Chem.* **2016**, *59*, 507−516.
(38) Cardiano, P.; Fazio, E.; Lazzara, G.; Manickam, S.; Milioto, S.; Neri, F.; Mineo, P. G.; Piperno, A.; Lo Schiavo, S. Highly Untangled Multiwalled Carbon Nanotube@Polyhedral Oligomeric Silsesquioxane Ionic Hybrids: Synthesis, Characterization and Nonlinear Optical Properties. *Carbon* **2015**, *86*, 325−337.
(39) Cardiano, P.; Lazzara, G.; Manickam, S.; Mineo, P.; Milioto, S.; Lo Schiavo, S. POSS-Tetraalkylammonium Salts: A New Class of Ionic Liquids. *Eur. J. Inorg. Chem.* **2012**, 5668−5676.
(40) Manickam, S.; Cardiano, P.; Mineo, P. G.; Lo Schiavo, S. Star-Shaped Quaternary Alkylammonium Polyhedral Oligomeric Silsesquioxane Ionic Liquids. *Eur. J. Inorg. Chem.* **2014**, 2704−2710.
(41) Castriciano, M. A.; Leone, N.; Cardiano, P.; Manickam, S.; Scolaro, L. M.; Lo Schiavo, S. A new supramolecular polyhedral oligomeric silsesquioxanes (POSS)-porphyrin nanohybrid: synthesis and spectroscopic characterization. *J. Mater. Chem. C* **2013**, *1*, 4746−4753.
(42) Amendola, V.; Bergamaschi, G.; Boiocchi, M.; Fabbrizzi, L.; Mosca, L. The Interaction of Fluoride with Fluorogenic Ureas: An On1−Off−On2 Response. *J. Am. Chem. Soc.* **2013**, *135*, 6345−6355.
(43) Costa, A. L.; Gomes, A. C.; Pillinger, M.; Gonçalves, I. S.; Sérgio Seixas de Melo, J. Controlling the Fluorescence Behavior of 1-Pyrenesulfonate by Cointercalation with a Surfactant in a Layered Double Hydroxide. *Langmuir* **2015**, *31*, 4769−4778.
(44) de Robillard, G.; Makni, O.; Cattey, H.; Andrieu, J.; Devillers, C. H. Towards sustainable synthesis of pyren-1-yl azoliums via electrochemical oxidative C-N coupling. *Green Chem.* **2015**, *17*, 4669−4679.
(45) Figueira-Duarte, T. M.; Müllen, K. Pyrene-Based Materials for Organic Electronics. *Chem. Rev.* **2011**, *111*, 7260−7314.
(46) Hollamby, M. J.; Danks, A. E.; Schnepp, Z.; Rogers, S. E.; Hart, S. R.; Nakanishi, T. Fluorescent Liquid Pyrene Derivative-in-Water Microemulsions. *Chem. Commun.* **2016**, *52*, 7344−7347.
(47) Strauß, J.; Daub, J. Donor−Acceptor Functionalized Luminescent Hairpin Peptides: Electrochemiluminescence of Pyrene/Phenothiazine-Substituted Optically Active Systems. *Adv. Mater.* **2002**, *14*, 1652−1655.
(48) Kalyanasundaram, K.; Thomas, J. K. Environmental Effects on Vibronic Band Intensities in Pyrene Monomer Fluorescence and Their Application in Studies of Micellar Systems. *J. Am. Chem. Soc.* **1977**, *99*, 2039−2044.
(49) Laguerre, A.; Stefan, L.; Larrouy, M.; Genest, D.; Novotna, J.; Pirrotta, M.; Monchaud, D. A Twice-as-Smart Synthetic G-Quartet: Pyrotasq Is Both a Smart Quadruplex Ligand and a Smart Fluorescent Probe. *J. Am. Chem. Soc.* **2014**, *136*, 12406−12414.
(50) Mohr, A.; Talbiersky, P.; Korth, H.-G.; Sustmann, R.; Boese, R.; Bläser, D.; Rehage, H. A New Pyrene-Based Fluorescent Probe for the Determination of Critical Micelle Concentrations. *J. Mater. Chem. B* **2007**, *111*, 12985−12992.
(51) Singh, M.; Holzinger, M.; Biloivan, O.; Cosnier, S. 3d-Nanostructured Scaffold Electrodes Based on Single-Walled Carbon Nanotubes and Nanodiamonds for High Performance Biosensors. *Carbon* **2013**, *61*, 349−356.
(52) Venkataramana, G.; Sankararaman, S. Synthesis and Spectroscopic Investigation of Aggregation through Cooperative $\pi-\pi$ and C−H···O Interactions in a Novel Pyrene Octaaldehyde Derivative†. *Org. Lett.* **2006**, *8*, 2739−2742.
(53) Winnik, F. M. Photophysics of Preassociated Pyrenes in Aqueous Polymer Solutions and in Other Organized Media. *Chem. Rev.* **1993**, *93*, 587−614.
(54) Endo, T.; Kato, T.; Tozaki, K.-i.; Nishikawa, K. Phase Behaviors of Room Temperature Ionic Liquid Linked with Cation Conformational Changes: 1-Butyl-3-Methylimidazolium Hexafluorophosphate. *J. Mater. Chem. B* **2010**, *114*, 407−411.
(55) Triolo, A.; Mandanici, A.; Russina, O.; Rodriguez-Mora, V.; Cutroni, M.; Hardacre, C.; Nieuwenhuyzen, M.; Bleif, H.-J.; Keller, L.; Ramos, M. A. Thermodynamics, Structure, and Dynamics in Room Temperature Ionic Liquids: The Case of 1-Butyl-3-methyl Imidazolium Hexafluorophosphate ([bmim][PF6]). *J. Mater. Chem. B* **2006**, *110*, 21357−21364.
(56) Yang, M.; Mallick, B.; Mudring, A.-V. On the Mesophase Formation of 1,3-Dialkylimidazolium Ionic Liquids. *Cryst. Growth Des.* **2013**, *13*, 3068−3077.
(57) Park, M.; Yoon, W.-J.; Kim, D.-Y.; Choi, Y.-J.; Koo, J.; Lim, S.-I.; Kang, D.-G.; Hsu, C.-H.; Jeong, K.-U. Pyrene-Based Asymmetric Supramolecule: Kinetically Controlled Polymorphic Superstructures by Molecular Self-Assembly. *Cryst. Growth Des.* **2017**, *17*, 1707−1715.
(58) Menger, F. M.; Whitesell, L. G. Binding Properties of 1-Pyrenesulfonic Acid in Water. *J. Org. Chem.* **1987**, *52*, 3793−3798.
(59) Lee, D.-W.; Kim, T.; Lee, M. An Amphiphilic Pyrene Sheet for Selective Functionalization of Graphene. *Chem. Commun.* **2011**, *47*, 8259−8261.
(60) Narayan, R.; Lim, J.; Jeon, T.; Li, D. J.; Kim, S. O. Perylene Tetracarboxylate Surfactant Assisted Liquid Phase Exfoliation of Graphite into Graphene Nanosheets with Facile Re-Dispersibility in Aqueous/Organic Polar Solvents. *Carbon* **2017**, *119*, 555−568.
(61) Viinikanoja, A.; Kauppila, J.; Damlin, P.; Mäkilä, E.; Leiro, J.; Ääritalo, T.; Lukkari, J. Interactions between Graphene Sheets and Ionic Molecules Used for the Shear-Assisted Exfoliation of Natural Graphite. *Carbon* **2014**, *68*, 195−209.
(62) Yang, H.; Hernandez, Y.; Schlierf, A.; Felten, A.; Eckmann, A.; Johal, S.; Louette, P.; Pireaux, J.-J.; Feng, X.; Mullen, K.; Palermo, V.; Casiraghi, C. A Simple Method for Graphene Production Based on Exfoliation of Graphite in Water Using 1-Pyrenesulfonic Acid Sodium Salt. *Carbon* **2013**, *53*, 357−365.
(63) Zhang, M.; Parajuli, R. R.; Mastrogiovanni, D.; Dai, B.; Lo, P.; Cheung, W.; Brukh, R.; Chiu, P. L.; Zhou, T.; Liu, Z.; Garfunkel, E.; He, H. Production of Graphene Sheets by Direct Dispersion with Aromatic Healing Agents. *Small* **2010**, *6*, 1100−1107.
(64) Matsumoto, M.; Saito, Y.; Park, C.; Fukushima, T.; Aida, T. Ultrahigh-throughput exfoliation of graphite into pristine 'single-layer' graphene using microwaves and molecularly engineered ionic liquids. *Nat. Chem.* **2015**, *7*, 730−736.
(65) Nuvoli, D.; Valentini, L.; Alzari, V.; Scognamillo, S.; Bon, S. B.; Piccinini, M.; Illescas, J.; Mariani, A. High Concentration Few-Layer Graphene Sheets Obtained by Liquid Phase Exfoliation of Graphite in Ionic Liquid. *J. Mater. Chem.* **2011**, *21*, 3428−3431.
(66) Wang, X.; Fulvio, P. F.; Baker, G. A.; Veith, G. M.; Unocic, R. R.; Mahurin, S. M.; Chi, M.; Dai, S. Direct Exfoliation of Natural Graphite into Micrometre Size Few Layers Graphene Sheets Using Ionic Liquids. *Chem. Commun.* **2010**, *46*, 4487−4489.
(67) Merlen, A.; Buijnsters, J.; Pardanaud, C. A Guide to and Review of the Use of Multiwavelength Raman Spectroscopy for Characterizing Defective Aromatic Carbon Solids: From Graphene to Amorphous Carbons. *Coatings* **2017**, *7*, 153.
(68) Wu, J.-B.; Lin, M.-L.; Cong, X.; Liu, H.-N.; Tan, P.-H. Raman Spectroscopy of Graphene-Based Materials and Its Applications in Related Devices. *Chem. Soc. Rev.* **2018**, *47*, 1822−1873.
(69) Wiercigroch, E.; Szafraniec, E.; Czamara, K.; Pacia, M. Z.; Majzner, K.; Kochan, K.; Kaczor, A.; Baranska, M.; Malek, K. Raman and Infrared Spectroscopy of Carbohydrates: A Review. *Spectrochim. Acta, Part A* **2017**, *185*, 317−335.
(70) Montaudo, G.; Scamporrino, E.; Vitalini, D.; Mineo, P. Novel Procedure for Molecular Weight Averages Measurement of Polydisperse Polymers Directly from Matrix-Assisted Laser Desorption/Ionization Time-of-Flight Mass Spectra. *Rapid Commun. Mass Spectrom.* **1996**, *10*, 1551−1559.
(71) Scamporrino, E.; Maravigna, P.; Vitalini, D.; Mineo, P. A New Procedure for Quantitative Correction of Matrix-Assisted Laser Desorption/Ionization Time-of-Flight Mass Spectrometric Response. *Rapid Commun. Mass Spectrom.* **1998**, *12*, 646−650.

DOI: 10.1021/acsomega.8b02961
ACS Omega 2018, 3, 18811−18820

(72) Vitalini, D.; Mineo, P.; Scamporrino, E. Further Application of a Procedure for Molecular Weight and Molecular Weight Distribution Measurement of Polydisperse Polymers from Their Matrix-Assisted Laser Desorption/Ionization Time-of-Flight Mass Spectra. *Macromolecules* **1997**, *30*, 5285−5289.
(73) Vitalini, D.; Mineo, P.; Scamporrino, E. Effect of Combined Changes in Delayed Extraction Time and Potential Gradient on the Mass Resolution and Ion Discrimination in the Analysis of Polydisperse Polymers and Polymer Blends by Delayed Extraction Matrix-Assisted Laser Desorption/Ionization Time-of-Flight Mass Spectrometry. *Rapid Commun. Mass Spectrom.* **1999**, *13*, 2511−2517.
(74) Mineo, P.; Vitalini, D.; Scamporrino, E.; Bazzano, S.; Alicata, R. Effect of Delay Time and Grid Voltage Changes on the Average Molecular Mass of Polydisperse Polymers and Polymeric Blends Determined by Delayed Extraction Matrix-Assisted Laser Desorption/Ionization Time-of-Flight Mass Spectrometry. *Rapid Commun. Mass Spectrom.* **2005**, *19*, 2773−2779.
(75) Pasternack, R.; Collings, P. Resonance Light Scattering: A New Technique for Studying Chromophore Aggregation. *Science* **1995**, *269*, 935−939.

DOI: 10.1021/acsomega.8b02961
ACS Omega 2018, 3, 18811−18820